PHILOSOPHICAL TRANSACTIONS OF THE ROYAL SOCIETY A MATHEMATICAL, PHYSICAL & ENGINEERING SCIENCES

A human ventricular cell model for investigation of cardiac arrhythmias under hyperkalaemic conditions

Jesús Carro, José Félix Rodríguez, Pablo Laguna and Esther Pueyo

Phil. Trans. R. Soc. A 2011 **369**, 4205-4232
doi: 10.1098/rsta.2011.0127

PHILOSOPHICAL TRANSACTIONS OF THE ROYAL SOCIETY A

Phil. Trans. R. Soc. A (2011) **369**, 4205–4232
doi:10.1098/rsta.2011.0127

A human ventricular cell model for investigation of cardiac arrhythmias under hyperkalaemic conditions

By Jesús Carro[1,2], José Félix Rodríguez[1], Pablo Laguna[1,2] and Esther Pueyo[1,2,*]

[1]*Aragón Institute of Engineering Research (I3A), IIS Aragón, Universidad de Zaragoza, Spain*
[2]*CIBER in Bioengineering, Biomaterials and Nanomedicine (CIBER-BBN), Zaragoza, Spain*

In this study, several modifications were introduced to a recently proposed human ventricular action potential (AP) model so as to render it suitable for the study of ventricular arrhythmias. These modifications were driven by new sets of experimental data available from the literature and the analysis of several well-established cellular arrhythmic risk biomarkers, namely AP duration at 90 per cent repolarization (APD_{90}), AP triangulation, calcium dynamics, restitution properties, APD_{90} adaptation to abrupt heart rate changes, and rate dependence of intracellular sodium and calcium concentrations. The proposed methodology represents a novel framework for the development of cardiac cell models. Five stimulation protocols were applied to the original model and the ventricular AP model developed here to compute the described arrhythmic risk biomarkers. In addition, those models were tested in a one-dimensional fibre in which hyperkalaemia was simulated by increasing the extracellular potassium concentration, $[K^+]_o$. The effective refractory period (ERP), conduction velocity (CV) and the occurrence of APD alternans were investigated. Results show that modifications improved model behaviour as verified by: (i) AP triangulation well within experimental limits (the difference between APD at 50 and 90 per cent repolarization being 78.1 ms); (ii) APD_{90} rate adaptation dynamics characterized by fast and slow time constants within physiological ranges (10.1 and 105.9 s); and (iii) maximum S1S2 restitution slope in accordance with experimental data ($S_{S1S2} = 1.0$). In simulated tissues under hyperkalaemic conditions, APD_{90} progressively shortened with the degree of hyperkalaemia, whereas ERP increased once a threshold in $[K^+]_o$ was reached ($[K^+]_o \approx 6$ mM). CV decreased with $[K^+]_o$, and conduction was blocked for $[K^+]_o > 10.4$ mM. APD_{90} alternans were observed for $[K^+]_o > 9.8$ mM. Those results adequately reproduce experimental observations. This study demonstrated the value of basing the development

*Author for correspondence (epueyo@unizar.es).

Electronic supplementary material is available at http://dx.doi.org/10.1098/rsta.2011.0127 or via http://rsta.royalsocietypublishing.org.

One contribution of 11 to a Theme Issue 'Towards the virtual physiological human: mathematical and computational case studies'.

of AP models on the computation of arrhythmic risk biomarkers, as opposed to joining together independently derived ion channel descriptions to produce a whole-cell AP model, with the new framework providing a better picture of the model performance under a variety of stimulation conditions. On top of replicating experimental data at single-cell level, the model developed here was able to predict the occurrence of APD_{90} alternans and areas of conduction block associated with high $[K^+]_o$ in tissue, which is of relevance for the investigation of the arrhythmogenic substrate in ischaemic hearts.

Keywords: electrophysiology; cardiac arrhythmias; human ventricular cell model; hyperkalaemia

1. Introduction

Mathematical modelling and simulation of the heart's electrical activity (so-called cardiac electrophysiology) and signal processing of bioelectrical signals provide an ideal framework to combine the information from clinical and experimental studies with the understanding of their underlying mechanisms. Tools capable of testing different hypotheses and predicting potential abnormalities in the heart's behaviour can be produced within that framework. In the relatively near future, it is not unlikely that those tools might even be used in clinical practice as complementary instruments to help in the prevention of cardiac diseases and the improvement of their diagnosis and therapy. Specifically, for the study of ventricular arrhythmias, it remains essential to have an action potential (AP) model able to reproduce experimentally and clinically observed arrhythmic behaviours at cell and tissue level. This would allow simulation of the electrical activity of the heart from the cell to the body surface and a total *in silico* reconstruction of the most well-known bioelectrical signal, the electrocardiogram, to be used for investigation of the mechanisms and manifestations of ventricular arrhythmias at different scales.

In the last few years, a number of mathematical models of electrical and ionic homeostasis in human ventricular myocytes have been proposed. One of the most extensively used models is the one proposed by ten Tusscher & Panfilov [1] (TP06), which is an improved version of the model described by ten Tusscher *et al.* [2] (TNNP04), where the calcium dynamics, the slow delayed rectifier potassium current (I_{Ks}) and the L-type calcium current (I_{CaL}) were reformulated. Both the TNNP04 and the TP06 models are based on experimental human data for most of the main ionic currents. One of the major advantages of the TP06 model against previous human ventricular models is that it accurately reproduces restitution of the AP duration (APD_{90}), as will be illustrated in §3 of this paper. On the other hand, the TP06 model has the major shortcomings of being insensitive to changes in certain ionic current densities [3] and of inadequately representing the rate dependence of intracellular calcium levels [4], which will also be verified in the present study. Another relevant model of human ventricular cells was proposed by Iyer *et al.* [5] (IMW04). That model provides a detailed description of calcium homeostasis and reproduces diverse aspects of the excitation–contraction coupling (ECC). However, important limitations have been reported for this model, including the fact that it is extremely sensitive to variations in the sodium–potassium pump ($I_{Na,K}$) and inward rectifier potassium

(I_{K1}) current densities [3] and that it produces very long APs and relatively flat restitution curves in tissues [6]. On top of that, the most relevant ionic currents in the IMW04 model are described using Markovian chains, with the consequent increase in complexity (more than 60 state variables), which imposes serious restrictions on the size of the time step required for stability and increases the overall computational time when using this model in tissue simulations [6]. Recently, a new model of human ventricular AP has been proposed by Grandi *et al.* [7] (GPB). The development of that model departs from the rabbit ECC model proposed by Shannon *et al.* [8], which includes the subsarcolemmal and junctional compartments in the formulation of the currents and provides a detailed description of calcium handling. The GPB model includes new definitions of ionic current densities and kinetics according to recent experimental data on human myocytes. This model is defined for two types of cells, namely endocardial and epicardial. The definitions of those two cell types differ only in the maximal conductivity of the fast and slow components of the transient outward potassium current (I_{to}). The GPB model improves the AP response to frequency changes and offers a better performance against blockades of potassium currents (I_{K1}, I_{Ks} and the rapid delayed rectifier potassium current I_{Kr}) with respect to the TP06 model. The major drawback of the GPB model is that it does not adequately reproduce S1S2 restitution properties nor APD_{90} rate adaptation dynamics, as will be illustrated in this study. Those drawbacks can be attributed to the fact that the GPB model was developed from a rabbit ventricular model, and the characteristics of S1S2 restitution and APD_{90} rate adaptation are notably different in the two species. Table 1 presents a summary with the main differences between the three models described above, i.e. TP06, IMW04 and GPB.

Despite the fact that the human ventricular AP models currently available in the literature are able to reproduce certain electrophysiological properties, they fail in representing other relevant aspects, as pointed out above. In order to obtain a model suitable for the study of ventricular arrhythmias, in this study a human ventricular AP model was developed that departs from the GPB model. The methodology followed for model development was based on the computation of well-established arrhythmic risk biomarkers and the results of a sensitivity analysis of the modulation of those biomarkers by variations in the main ionic currents. Using that methodology, key limitations of the GPB model were unravelled and inadequacies in the definitions of specific ionic current characteristics were identified. Based on those findings, gating kinetics of the I_{CaL} current were reformulated by introducing both fast and slow voltage-dependent inactivation gates [1], maximal $I_{Na,K}$ was reduced to best match the experimental APD_{90} rate adaptation data and the I_{K1} current was redefined by accounting for recent experimental data published in the literature [9]. The new model, developed by Carro *et al.* in this paper (CRLP), was tested and compared with the original GPB model and with the widely used TP06 model. The IMW04 model was left out of the comparison because of the limitations pointed out above. Model comparison was based on 12 cellular arrhythmic risk biomarkers computed using five different stimulation protocols, as in Romero *et al.* [4]. Our results show that the introduced modifications brought most biomarkers into the physiological range, and considerably improved others with respect to the GPB and the TP06 models. In addition, the CRLP

Table 1. Differences between human ventricular cell models. Data are obtained from Niederer *et al.* [3], Romero *et al.* [4] and Bueno-Orovio *et al.* [6] and from simulations performed in this study.

	TP06	IMW04	GPB
state variables	20	67	38
computation time	short	very long	long
cell types	endo, mid, epi	epi	endo, epi
steady-state AP properties	physiological APD values, very low triangulation	physiological APD values and triangulation	physiological APD values and triangulation
steady-state calcium levels	low diastolic and systolic values	low diastolic and systolic values	very low diastolic and systolic values
APD_{90} adaptation to abrupt heart rate changes	very fast	very slow	rabbit characteristics
sodium and calcium rate dependence	very sensitive to increasing stimulation frequency	physiological behaviour	physiological behaviour
APD sensitivity to variations in ionic current densities	less sensitive to $I_{Na,K}$, $I_{Na,Ca}$, I_{Ks}, I_{K1}, I_{CaL}, I_{Kr} and I_{Na}	highly sensitive to $I_{Na,K}$ and I_{K1}	less sensitive to I_{Kr} and highly sensitive to I_{K1}

model was tested by simulating hyperkalaemic conditions in tissues. Under those conditions, potassium starts to pour out of ischaemic myocardial cells, causing depolarization of the myocardium at rest, slowing conduction and decreasing excitability. Recovery of excitability is known to outlast repolarization, a phenomenon termed post-repolarization refractoriness. Our results show that under hyperkalaemia APD_{90} progressively decreased with the level of extracellular potassium, $[K^+]_o$, whereas the effective refractory period (ERP) increased after a threshold in the level of $[K^+]_o$ was surpassed. Conduction velocity (CV) decreased with $[K^+]_o$ and conduction was blocked above $[K^+]_o = 10.4\,\text{mM}$. Additionally, APD_{90} alternans appeared for $[K^+]_o > 9.8\,\text{mM}$. These results suggest that the model is suitable to represent areas of inhomogeneities of resting potential and dispersion in the recovery of excitability corresponding to different hyperkalaemic levels within the tissue. Those areas of inhomogeneities could provide a setting for unidirectional block that could become the substrate for arrhythmias in ischaemic hearts.

2. Methods

(a) Model development

In this study, a human ventricular cell model was developed that departs from the recently proposed GPB model. Before describing the modifications introduced into the new model, a brief description of the GPB model is in order.

(i) *The GPB model*

The GPB model describes the AP of endocardial and epicardial human myocytes. For both cell types, the total transmembrane ionic current, I_{ion}, is given by

$$I_{\mathrm{ion}} = I_{\mathrm{Na_{tot}}} + I_{\mathrm{Cl_{tot}}} + I_{\mathrm{Ca_{tot}}} + I_{\mathrm{K_{tot}}},$$

where each of the individual currents denotes the current generated on passing sodium, chlorine, calcium and potassium ions through the cell membrane, respectively.

Sodium current. Following the approach of Shannon *et al.* [8], the sodium current was divided into two components: (i) a subsarcolemmal component and (ii) a junctional component, which correspond to the cell compartments where the current is generated. Both components are formed by the same subcurrents:

$$I_{\mathrm{Na_{tot_{junc}}}} = I_{\mathrm{Na_{junc}}} + I_{\mathrm{NaBk_{junc}}} + 3I_{\mathrm{ncx_{junc}}} + 3I_{\mathrm{Na,K_{junc}}} + I_{\mathrm{Ca_{Na_{junc}}}},$$

$$I_{\mathrm{Na_{tot_{sl}}}} = I_{\mathrm{Na_{sl}}} + I_{\mathrm{NaBk_{sl}}} + 3I_{\mathrm{ncx_{sl}}} + 3I_{\mathrm{Na,K_{sl}}} + I_{\mathrm{Ca_{Na_{sl}}}}$$

and

$$I_{\mathrm{Na_{tot}}} = I_{\mathrm{Na_{tot_{junc}}}} + I_{\mathrm{Na_{tot_{sl}}}},$$

where I_{Na} is the fast sodium current, I_{NaBk} is the background sodium current, I_{ncx} is the current of the sodium–calcium exchanger, $I_{\mathrm{Na,K}}$ is the current of the sodium–potassium pump and $I_{\mathrm{Ca_{Na}}}$ is the sodium current through the L-type calcium channels.

Chlorine current. The chlorine current, which is not present in the TP06 model, is described in the GPB model by

$$I_{\mathrm{Cl_{tot}}} = I_{\mathrm{ClCa}} + I_{\mathrm{ClBk}},$$

where I_{ClCa} is the calcium-activated chlorine current, and I_{ClBk} is the background chlorine current.

Calcium current. The calcium current, as in the case of the sodium current, has two components, junctional and subsarcolemmal:

$$I_{\mathrm{Ca_{tot_{junc}}}} = I_{\mathrm{Ca_{junc}}} + I_{\mathrm{CaBk_{junc}}} + I_{\mathrm{pCa_{junc}}} - 2I_{\mathrm{ncx_{junc}}},$$

$$I_{\mathrm{Ca_{tot_{sl}}}} = I_{\mathrm{Ca_{sl}}} + I_{\mathrm{CaBk_{sl}}} + I_{\mathrm{pCa_{sl}}} - 2I_{\mathrm{ncx_{sl}}}$$

and

$$I_{\mathrm{Ca_{tot}}} = I_{\mathrm{Ca_{tot_{junc}}}} + I_{\mathrm{Ca_{tot_{sl}}}},$$

where I_{Ca} is the calcium current through the L-type calcium channels, I_{CaBk} is the background calcium current, I_{pCa} is the sarcolemmal calcium pump current and I_{ncx} is the current of the sodium–calcium exchanger.

Potassium current. The potassium current is defined as

$$I_{\mathrm{K_{tot}}} = I_{\mathrm{to}} + I_{\mathrm{Kr}} + I_{\mathrm{Ks}} + I_{\mathrm{K1}} - 2I_{\mathrm{Na,K}} + I_{\mathrm{Ca_K}} + I_{\mathrm{Kp}},$$

where I_{to} is the transient outward potassium current (decomposed into a fast and a slow component), I_{Kr} is the rapidly activating potassium current, I_{Ks} is the slowly activating potassium current (decomposed into junctional and subsarcolemmal components), I_{K1} is the inward rectifier potassium current, $I_{\mathrm{Na,K}}$ is the current of the sodium–potassium pump (decomposed into junctional and subsarcolemmal components), $I_{\mathrm{Ca_K}}$ is the potassium current through the L-type calcium channels (decomposed into junctional and subsarcolemmal components)

and I_{Kp} is the plateau potassium current. In the GPB model, differentiation between endocardial and epicardial cells is set by assigning different contributions to the fast and slow I_{to} components.

(ii) *The CRLP model*

Taking the GPB model as a starting point, the CRLP model was built by reformulating two ionic currents (I_{CaL} and I_{K1}) and redefining a number of model parameters, including G_{Na} (maximum I_{Na} conductance) and $G_{Na,K}$ (maximal $I_{Na,K}$ value). Those changes were motivated by the poor performance exhibited by the GPB model on two particular aspects: (i) the shape and slope of the S1S2 APD_{90} restitution curve, and (ii) the response of the APD_{90} to abrupt changes in heart rate (see below). The failure of the GPB model in reproducing experimental data on those two aspects could be attributed to an inheritance from the Shannon rabbit ventricular model from which the GPB model was developed. In this regard, the development of the CRLP model from the GPB model was made by considering human data only [3]. The following paragraphs describe the introduced modifications, as well as the data and criteria used in the development process. A full description of the CRLP model along with a CellML implementation of it can be found in the electronic supplementary material.

In order to maintain as much consistency as possible with the original GPB model, the CRLP model was developed for the same type of myocardial cells as the GPB model, namely endocardial and epicardial. Differentiation between the two cell types was based on the definition of the I_{to} fast and slow components, in the same way as previously described for the GPB model.

L-type calcium current (I_{CaL}). In order to obtain an APD_{90} adaptation response to abrupt changes in cycle length (CL) in better concordance with experimental data, the L-type calcium current was reformulated. The voltage-dependent inactivation gate f of the GPB model was replaced with the product of a fast, f, and a slow, f_2, inactivation gate, as in ten Tusscher *et al.* [1]. The new equations for the L-type current in the CRLP model are

$$I_{Ca_{junc}} = F_{junc_{Ca_L}} \times \bar{I}_{Ca_j} \times d \times f \times f_2(1 - f_{Ca_{B_j}}),$$

$$I_{Ca_{sl}} = F_{sl_{Ca_L}} \times \bar{I}_{Ca_{sl}} \times d \times f \times f_2(1 - f_{Ca_{B_{sl}}}),$$

$$I_{Ca_{Na_{junc}}} = F_{junc_{Ca_L}} \times \bar{I}_{Na_j} \times d \times f \times f_2(1 - f_{Ca_{B_j}}),$$

$$I_{Ca_{Na_{sl}}} = F_{sl_{Ca_L}} \times \bar{I}_{Na_{sl}} \times d \times f \times f_2(1 - f_{Ca_{B_{sl}}}),$$

$$I_{Ca_K} = \bar{I}_K \times d \times f \times f_2(F_{junc_{Ca_L}} \times (1 - f_{Ca_{B_j}}) + F_{sl_{Ca_L}} \times (1 - f_{Ca_{B_{sl}}})),$$

$$I_{Ca} = I_{Ca_{junc}} + I_{Ca_{sl}},$$

$$I_{Ca_{Na}} = I_{Ca_{Na_{junc}}} + I_{Ca_{Na_{sl}}}$$

and

$$I_{CaL} = I_{Ca} + I_{Ca_K} + I_{Ca_{Na}}.$$

As indicated in Niederer *et al.* [3], the replacement of one current component by another one is not a simple task. Splitting the f gate in the GPB model into two new gates required the readjustment of the time constants τ_{f_2} associated with the slow voltage-dependent inactivation gate f_2 and the time constant τ_d associated

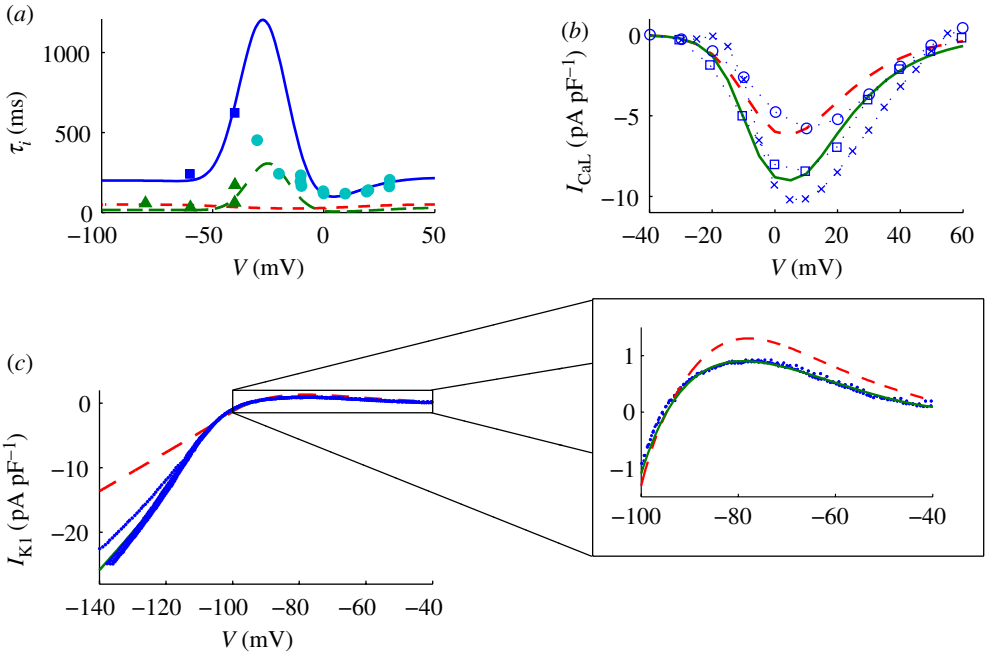

Figure 1. Characteristics of I_{CaL} and I_{K1} in simulations and experiments. (*a*) Simulated I_{CaL} voltage-dependent inactivation time constants τ_i as a function of voltage, where $i \in \{f, f_2\}$. Experimental data, represented by symbols, were taken from [10–14] (blue full line, τ_f CRLP; green dashed line, τ_{f_2} CRLP; red dashed line, τ_f GPB; filled light blue circles, inactivation; filled dark blue squares, slow inactivation; filled green triangles, fast inactivation). (*b*) I_{CaL} current density versus voltage, with experimental data taken from [14–16] (red dashed line, GPB; green full line, CRLP; open blue circles, [15]; open blue squares, [14]; crosses, [16]). (*c*) I_{K1} current density versus voltage, with experimental data taken from [9] (red dashed line, GPB; green full line, CRLP; blue dotted line, [9]). To compare simulated and experimental data under the same conditions, $[K^+]_i = 138$ mM and $[K^+]_o = 4$ mM were used for the curves shown in (*c*), with $[K^+]_i$ denoting the intracellular potassium concentration. (Online version in colour.)

with the activation gate d in order to obtain a meaningful I_{CaL} current–voltage curve (splitting the f gate without readjusting the time constants would have led to a current–voltage curve having two relative minima).

Readjustment of τ_{f_2} was based on available experimental data [10–14]. Figure 1*a* depicts τ_f and τ_{f_2} along with experimental data [10–14]. Since the experimental data do not cover the entire voltage range, the readjustment was performed by best fitting the tail of the τ_{f_2} curve while obtaining a current–voltage curve within the range of experimental data. The other voltage-dependent inactivation time constant, τ_f, was kept as in the study of ten Tusscher *et al.* [1]. The equations describing f and f_2 are:

$$f_{ss} = \frac{1}{1 + e^{(V_m+20)/7}},$$

$$\alpha_f = 1102.5\, e^{-((V_m+27)/15)^2},$$

$$\beta_f = \frac{200}{1 + e^{(13-V_m)/10}},$$

$$\gamma_f = \frac{180}{1 + \mathrm{e}^{(V_\mathrm{m}+30)/10}} + 20,$$

$$\tau_f = \alpha_f + \beta_f + \gamma_f,$$

$$\frac{\mathrm{d}f}{\mathrm{d}t} = \frac{f_\mathrm{ss} - f}{\tau_f},$$

$$f_{2_\mathrm{ss}} = \frac{0.67}{1 + \mathrm{e}^{(V_\mathrm{m}+35)/7}} + 0.33,$$

$$\alpha_{f_2} = 300\,\mathrm{e}^{-(V_\mathrm{m}+25)^2/170},$$

$$\beta_{f_2} = \frac{31}{1 + \mathrm{e}^{(25-V_\mathrm{m})/10}},$$

$$\gamma_{f_2} = \frac{16}{1 + \mathrm{e}^{(V_\mathrm{m}+30)/10}},$$

$$\tau_{f_2} = \alpha_{f_2} + \beta_{f_2} + \gamma_{f_2}$$

and

$$\frac{\mathrm{d}f_2}{\mathrm{d}t} = \frac{f_{2_\mathrm{ss}} - f_2}{\tau_{f_2}},$$

where V_m denotes transmembrane voltage.

Readjustment of τ_d was based on the description provided in ten Tusscher *et al.* [1]:

$$d_\mathrm{ss} = \frac{1}{1 + \mathrm{e}^{-(V_\mathrm{m}+5)/6}},$$

$$\alpha_\mathrm{d} = \frac{1.4}{1 + \mathrm{e}^{(-35-V_\mathrm{m})/13}} + 0.25,$$

$$\beta_\mathrm{d} = \frac{1.4}{1 + \mathrm{e}^{(V_\mathrm{m}+5)5}},$$

$$\gamma_\mathrm{d} = \frac{1}{1 + \mathrm{e}^{(50-V_\mathrm{m})20}},$$

$$\tau_\mathrm{d} = \alpha_\mathrm{d}\beta_\mathrm{d} + \gamma_\mathrm{d}$$

and

$$\frac{\mathrm{d}d}{\mathrm{d}t} = \frac{d_\mathrm{ss} - d}{\tau_\mathrm{d}}.$$

The definitions of the calcium-dependent inactivation gates, $f_{\mathrm{Ca}_{\mathrm{B}_j}}$ and $f_{\mathrm{Ca}_{\mathrm{B}_\mathrm{sl}}}$, were taken as in the GPB model:

$$\frac{\mathrm{d}f_{\mathrm{Ca}_{\mathrm{B}_j}}}{\mathrm{d}t} = 1.7\,\mathrm{Ca}_j(1 - f_{\mathrm{Ca}_{\mathrm{B}_j}}) - 11.9 \times 10^{-3} f_{\mathrm{Ca}_{\mathrm{B}_j}}$$

and

$$\frac{\mathrm{d}f_{\mathrm{Ca}_{\mathrm{B}_\mathrm{sl}}}}{\mathrm{d}t} = 1.7\,\mathrm{Ca}_\mathrm{sl}\,(1 - f_{\mathrm{Ca}_{\mathrm{B}_\mathrm{sl}}}) - 11.9 \times 10^{-3} f_{\mathrm{Ca}_{\mathrm{B}_\mathrm{sl}}}.$$

Additionally, based on the results of the sensitivity of APD_{90} to variations in the maximal I_CaL conductivity and the actual APD_{90} value in the GPB model

(see later tables), the relative permeabilities of the L-type calcium channels were set to:

$$p_{\mathrm{Ca}} = 1.9887 \times 10^{-4}\,\mathrm{cm\,s^{-1}},$$
$$p_{\mathrm{K}} = 5.4675 \times 10^{-8}\,\mathrm{cm\,s^{-1}},$$
$$p_{\mathrm{Na}} = 3.0375 \times 10^{-9}\,\mathrm{cm\,s^{-1}},$$
$$\bar{I}_{\mathrm{Ca}_j} = \frac{p_{\mathrm{Ca}} \times V_{\mathrm{m}} \times \mathrm{Frdy} \times \mathrm{FoRT}(\mathrm{Ca}_j \times \mathrm{e}^{2V_{\mathrm{m}} \times \mathrm{FoRT}} - \mathrm{Ca}_{\mathrm{o}})}{\mathrm{e}^{2V_{\mathrm{m}} \times \mathrm{FoRT}} - 1},$$
$$\bar{I}_{\mathrm{Ca}_{\mathrm{sl}}} = \frac{p_{\mathrm{Ca}} \times V_{\mathrm{m}} \times \mathrm{Frdy} \times \mathrm{FoRT}(\mathrm{Ca}_{\mathrm{sl}} \times \mathrm{e}^{2V_{\mathrm{m}} \times \mathrm{FoRT}} - \mathrm{Ca}_{\mathrm{o}})}{\mathrm{e}^{2V_{\mathrm{m}} \times \mathrm{FoRT}} - 1},$$
$$\bar{I}_{\mathrm{Na}_j} = \frac{p_{\mathrm{Na}} \times V_{\mathrm{m}} \times \mathrm{Frdy} \times \mathrm{FoRT}(\mathrm{Na}_j \times \mathrm{e}^{V_{\mathrm{m}} \times \mathrm{FoRT}} - \mathrm{Na}_{\mathrm{o}})}{\mathrm{e}^{V_{\mathrm{m}} \times \mathrm{FoRT}} - 1},$$
$$\bar{I}_{\mathrm{Na}_{\mathrm{sl}}} = \frac{p_{\mathrm{Na}} \times V_{\mathrm{m}} \times \mathrm{Frdy} \times \mathrm{FoRT}(\mathrm{Na}_{\mathrm{sl}} \times \mathrm{e}^{V_{\mathrm{m}} \times \mathrm{FoRT}} - \mathrm{Na}_{\mathrm{o}})}{\mathrm{e}^{V_{\mathrm{m}} \times \mathrm{FoRT}} - 1}$$

and

$$\bar{I}_{\mathrm{K}} = \frac{p_{\mathrm{K}} \times V_{\mathrm{m}} \times \mathrm{Frdy} \times \mathrm{FoRT}(K_i \times \mathrm{e}^{V_{\mathrm{m}} \times \mathrm{FoRT}} - K_{\mathrm{o}})}{\mathrm{e}^{V_{\mathrm{m}} \times \mathrm{FoRT}} - 1},$$

where Frdy is Faraday's constant, FoRT is the ratio between Faraday's constant and the product of the gas constant and the absolute temperature, $\bar{I}_{k_m}$ is the maximal current for ion k in the compartment m, and p_k is the relative permeability of ion k.

The current–voltage curve obtained with the new definition of the I_{CaL} current was compared with the experimental data [14–16] and with the original definition of the GPB model. Figure 1*b* shows the different current–voltage curves, where it can be observed that the new definition of I_{CaL} is in good agreement with the available experimental data [14–16], with the additional benefit of contributing to physiological model response in terms of S1S2 APD_{90} restitution and APD_{90} rate adaptation dynamics.

Inward rectifier K current (I_{K1}). The I_{K1} current was redefined using recent experimental data from human ventricular cells published in the literature [9]. The new definition for I_{K1} is as follows:

$$a_{\mathrm{K1}} = \frac{4.094}{1.0 + \mathrm{e}^{0.1217(V_{\mathrm{m}} - E_{\mathrm{K}} - 49.934)}},$$
$$b_{\mathrm{K1}} = \frac{15.720\ \mathrm{e}^{0.0674(V_{\mathrm{m}} - E_{\mathrm{K}} - 3.257)} + \mathrm{e}^{0.0618(V_{\mathrm{m}} - E_{\mathrm{K}} - 594.31)}}{1.0 + \mathrm{e}^{-0.1629(V_{\mathrm{m}} - E_{\mathrm{K}} + 14.207)}},$$
$$K1_{\mathrm{ss}} = \frac{a_{\mathrm{K1}}}{a_{\mathrm{K1}} + b_{\mathrm{K1}}}$$

and

$$I_{\mathrm{K1}} = 0.5715 \sqrt{\frac{[\mathrm{K}^+]_{\mathrm{o}}}{5.4}} \times \mathrm{K1}_{\mathrm{ss}}(V_{\mathrm{m}} - E_{\mathrm{K}}),$$

where E_{K} is the $[\mathrm{K}^+]$ reversal potential. Figure 1*c* shows the modified I_{K1} current compared with the experimental data from [9] and with I_{K1} from the GPB model.

Na/K pump current ($I_{Na,K}$). In order to improve the APD_{90} adaptation response to abrupt changes in CL, maximal $I_{Na,K}$ was reduced by 45 per cent with respect to its value in the GPB model. That reduction was set based on the results of the sensitivity analysis for the τ_{slow} biomarker that will be described below.

$[K^+]_i$ *and* G_{Na}. A more physiological value for $[K^+]_i$ of 138 mM was used in our model. Considering this value for $[K^+]_i$ makes the model more excitable when compared with the original GPB model because of the increased availability of sodium channels. Therefore, in order to obtain physiological values for the maximal upstroke velocity, dV/dt, in tissue, the maximum conductance of the sodium current, G_{Na}, was reduced to $18.864\,mS\,\mu F^{-1}$. This modification led to a maximal upstroke velocity of $228\,mV\,ms^{-1}$ in the simulated one-dimensional tissue (see below), which is in good agreement with the experimental results from [17].

(iii) *Numerical methods and implementation*

The cell membrane was modelled as an electrical circuit [18]. Mathematically, the transmembrane voltage V_m was described by the following ordinary differential equation:

$$C_m \frac{dV_m}{dt} = -(I_{ion} - I_{stim}), \tag{2.1}$$

where t is time, I_{ion} is the sum of all transmembrane ionic currents, I_{stim} is the externally applied stimulation current and C_m is the cell capacitance per unit surface area.

Propagation of the electrical activity in a one-dimensional fibre was described by the following parabolic reaction–diffusion equation [19]:

$$C_m \frac{\partial V_m}{\partial t} = -(I_{ion} - I_{stim}) + \frac{\partial}{\partial x}\left(\sigma \frac{\partial V}{\partial x}\right), \tag{2.2}$$

where σ is the diffusion coefficient of the tissue and x denotes the coordinate along the fibre.

Physical units in the model are as follows: time t is given in milliseconds, transmembrane potential V_m in millivolts, current densities in picoamperes per picofarad, and ionic concentrations in millimoles per litre.

The GPB and CRLP models were implemented in Fortran based on the original codes provided by Eleonora Grandi. The TP06 model was also implemented in Fortran from the original C codes available at Kirsten ten Tusscher's web page: www-binf.bio.uu.nl/khwjtuss. A CellML implementation of the CRLP model is available in the electronic supplementary material.

Cells and tissues were stimulated with square transmembrane current pulses twice the diastolic threshold in amplitude and 1 ms duration. For single-cell simulations, forward Euler integration with a time step $\Delta t = 0.002$ ms was used to integrate the system of differential equations governing the cellular electrical behaviour. For the one-dimensional simulations, a homogeneous 4 cm long fibre composed of epicardial cells was considered. A semi-implicit operator-splitting scheme [20] was used to solve equation (2.2) with a space discretization of $\Delta x = 0.1$ mm and a time step of $\Delta t = 0.002$ ms. A value of $\sigma = 0.0013\ cm^2\,ms^{-1}$ was used, corresponding to a maximum CV of $74\,cm\,s^{-1}$, which is in agreement

with experimentally reported CV values [21]. The cell capacitance was set to $C_m = 1\,\mu F\,cm^{-2}$. Five positions within the fibre were selected for further analysis in each simulation. Those positions were located at 1.5, 1.75, 2, 2.25 and 2.5 cm from the stimulation end of the cable. Reported APD_{90} and CV values were computed as mean values over those positions. In all cases, the Rush and Larsen integration scheme [22] was used to integrate the Hodgkin–Huxley type equations for the gating variables of the various time-dependent currents (m, h and j for I_{Na}; x_{to_f}, x_{to_s}, y_{to_f} and y_{to_s} for I_{to}; x_{kr} for I_{Kr}; x_{ks} for I_{Ks}; and d, f and f_2 for I_{CaL}).

In order to test the sensitivity of the numerical solution to the time and space discretization indicated above, simulations were performed using a time increment of 0.5 µs and a spatial discretization of 0.05 mm. Differences of less than 0.2 per cent for the steady-state biomarkers computed in isolated cells were obtained when compared with the default time and space steps used in this study. In tissues, CV and APD_{90} varied by less than 1.5 and 0.02 per cent, respectively. Also, other stimulus durations (from 1 to 3 ms) and amplitudes (from 1.5 to 2 times the diastolic threshold) were tested and confirmed to provide very similar results (differences in terms of APD_{90}, maximal upstroke velocity as well as CV in tissues were in all cases below 0.2%, 1.6% and 0.8%, respectively).

(*b*) *Arrhythmic risk biomarkers and stimulation protocols*

Arrhythmic risk biomarkers were used in this study to guide the modifications applied to the GPB model to produce the CRLP model. Specifically, biomarkers related to S1S2 restitution and APD_{90} rate adaptation dynamics were identified as not being adequately reproduced by the GPB model, and appropriate modifications (described in the previous section) were performed. Those and other biomarkers were also used to evaluate the performance of the CRLP model and compare it with that of the TP06 and GPB models.

In the following subsections, the cellular arrhythmic risk biomarkers used in this study are presented, and the protocols used to compute them are described.

(i) *Selected biomarkers*

— *APD_{90}*: APD has been traditionally considered as the main preclinical marker of drug cardiotoxicity. APD prolongation has been linked to long Q–T syndrome and increased risk of developing *torsades de pointes* [23,24]. APD_{90} is used in this study to denote AP duration at 90 per cent repolarization (figure 2*a*).

— *Triangulation*: this biomarker quantifies the shape of the final part of the AP, and is calculated as the difference between APD at 50 and 90 per cent repolarization (figure 2*a*). Low triangulation values indicate square APs, while high values indicate triangular APs. Triangulation has been proposed as a marker of pro-arrhythmia [23], with long APD_{90} values without triangular APs considered as anti-arrhythmic, and triangular APs considered as pro-arrhythmic in general.

— *Systolic and diastolic intracellular calcium* ($[Ca^{2+}]_i$) *levels*: calcium transient properties evaluated at different frequencies have been reported as risk markers [25,26]. In this study, diastolic (level at rest) and systolic (level at peak) calcium transient levels were evaluated at 0.5 and 1 Hz, respectively (figure 2*b*).

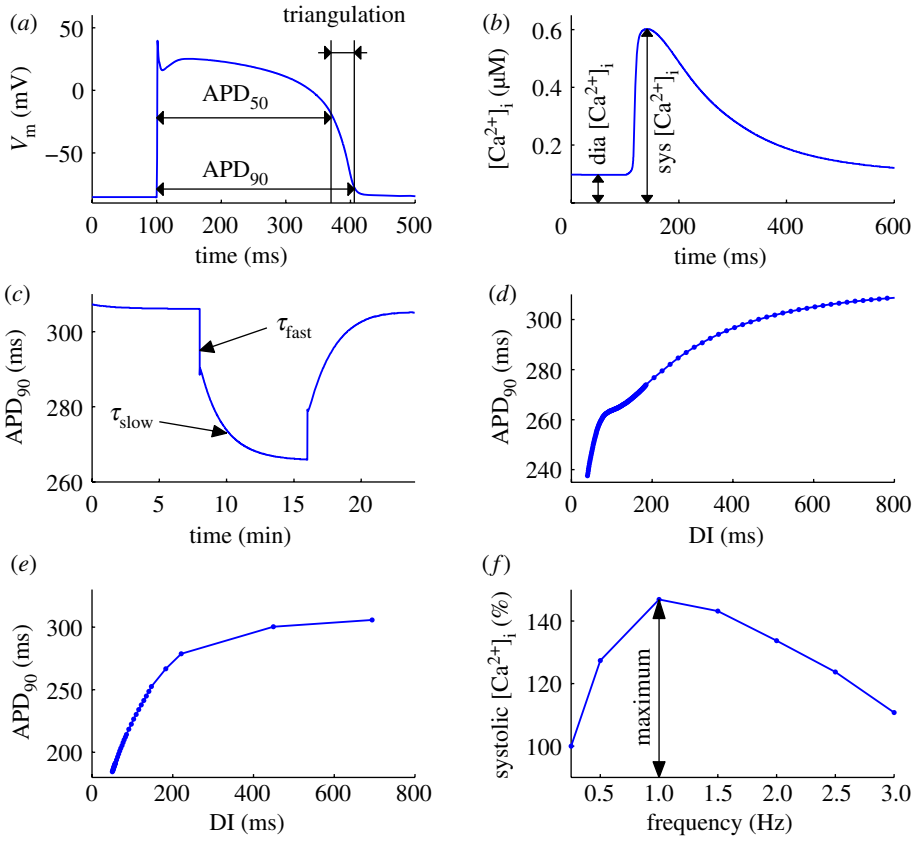

Figure 2. Graphical description (using simulation results) of the biomarkers of arrhythmic risk used in this study: (*a*) steady-state AP properties (APD_{90}, AP triangulation); (*b*) steady-state $[Ca^{2+}]_i$ properties (systolic 'sys' and diastolic 'dia' values); (*c*) APD_{90} adaptation to abrupt changes in CL (from 1000 to 600 ms and again to 1000 ms), characterized by time constants τ_{fast} and τ_{slow}; (*d*) APDR curve computed using the S1S2 protocol; (*e*) APDR curve computed using the dynamic protocol; and (*f*) normalized rate dependence of systolic concentrations, with normalization performed with respect to the lowest tested frequency, i.e. 0.25 Hz. For a better understanding of the protocols used to compute the biomarkers shown in (*a–f*), see the description provided in §2*b*(ii). (Online version in colour.)

— *Time constants of APD_{90} adaptation to abrupt changes in CL*: adaptation of ventricular repolarization duration to abrupt changes in CL has been proposed as an arrhythmic risk marker [27]. In this study, the dynamics of APD_{90} adaptation to abrupt changes in CL were fitted by two exponentials with associated time constants τ_{fast} and τ_{slow} (figure 2*c*), following the methodology proposed in Pueyo *et al.* [28].

— *Maximum slope of APD_{90} restitution curves*: the maximum slope of the APD_{90} restitution (APDR) curve has been suggested as an arrhythmic risk marker [29,30]. The APDR curve describes the relationship between APD_{90} and the diastolic interval (DI) (figure 2*d–e*). In this study, APDR was evaluated using the S1S2 and the dynamic protocols (see §2*b*(ii)).

— *Rate dependence of* Na^+ *and* Ca^{2+} *concentrations*: the importance of intracellular sodium, $[Na^+]_i$, and intracellular calcium, $[Ca^{2+}]_i$, dynamics in arrhythmogenesis has been extensively reported [31,32]. In this study, systolic $[Na^+]_i$ and $[Ca^{2+}]_i$ levels were evaluated for increasing stimulation frequencies (figure 2*f*).

(ii) *Stimulation protocols*

Five stimulation protocols were applied to evaluate the risk biomarkers presented in §2*b*(i).

— *Steady-state protocol*: a train of 3000 stimulation pulses was delivered and steady state was guaranteed to be reached. Simulations were carried out using two different CL values (1000 and 2000 ms). The evaluated biomarkers were: APD_{90} at 1 Hz, triangulation at 1 Hz, systolic $[Ca^{2+}]_i$ at 0.5 and 1 Hz and diastolic $[Ca^{2+}]_i$ at 0.5 and 1 Hz (figure 2*a*,*b*).
— *Abrupt changes in CL protocol*: the cell was stimulated with a CL of 1000 ms for 8 min, then with a CL of 600 ms for an additional 8 min and finally with a CL of 1000 ms for 8 min (figure 2*c*). The APD_{90} dynamics after the first abrupt CL change were fitted by two exponentials with time constants τ_{fast} and τ_{slow}. APD_{90} adaptation dynamics after the second abrupt CL change provided very similar results to those obtained for the first CL change, in accordance with earlier studies [4,28], and are not reported.
— *S1S2 protocol*: a train of 10 basic stimulations (S1) were applied to the cell or tissue at a CL of 1000 ms followed by an extra stimulus (S2) delivered at coupling intervals (CI) ranging from 1000 to 250 ms in variable steps (100 ms for DI > 300 ms, 5 ms for 150 < DI < 300 ms and 1 ms for 5 < DI < 150 ms). The S1S2 restitution curve was obtained by plotting the APD_{90} corresponding to the extra stimulus versus the previous DI for each of the tested CI values (figure 2*d*).
— *Dynamic protocol*: in this protocol, 100 stimulations were applied at a given CL, with the CL ranging from 1000 to 50 ms. The APDR curve was obtained by plotting the steady-state APD_{90} (corresponding to the 100th stimulus of each CL) versus the corresponding steady-state DI (figure 2*e*).
— *Rate-dependence protocol*: the systolic values of both $[Na^+]_i$ and $[Ca^{2+}]_i$ concentrations were measured at different frequencies (0.25, 0.5, 1, 1.5, 2, 2.5 and 3 Hz) and normalized to the level of the minimum frequency. For each frequency, the cell was stimulated during 10 min to reach steady state and $[Na^+]_i$ and $[Ca^{2+}]_i$ were measured at the end of the 10 min period. The maximum normalized concentration value was computed and used as a biomarker (figure 2*f*).

(*c*) *Conducted simulations*

(i) *Sensitivity analysis*

A sensitivity analysis was performed using the original GPB model following the methodology described in Romero *et al.* [4]. The aim was to elucidate how different ionic current properties modulate the investigated arrhythmic risk

biomarkers. In the sensitivity analysis, each parameter was varied one at a time by ±30%. Also, variations of ±15% were considered to assess biomarkers' response to different degrees of variation. These percentages are in agreement with variability levels reported in experiments performed in human ventricular tissue [9,14,33–37].

The following parameters were considered in the sensitivity analysis.

— G_{CaL}: maximal conductance of the L-type calcium current (I_{CaL}).
— τ_{f}: time constant of the fast voltage-dependent inactivation gate (f) of the I_{CaL} current.
— τ_{f2}: time constant of the slow voltage-dependent inactivation gate (f_2) of the I_{CaL} current.
— G_{Kr}: maximal conductance of the rapidly activating potassium current (I_{Kr}).
— G_{Ks}: maximal conductance of the slowly activating potassium current (I_{Ks}).
— τ_{xs}: time constant of the activation gate (x_{Ks}) of the I_{Ks} current.
— G_{K1}: maximal conductance of the inward rectifier potassium current (I_{K1}).
— $G_{\mathrm{Na,K}}$: maximal value of the sodium–potassium pump current ($I_{\mathrm{Na,K}}$).
— G_{ncx}: maximal value of the sodium–calcium exchanger current (I_{ncx}).
— G_{to}: maximal conductance of the transient outward potassium current (I_{to}).

For each biomarker c and parameter p, the percentage of change ($D_{c,p,a}$) and sensitivity ($S_{c,p,a}$) was calculated as follows [4]:

$$D_{c,p,a} = \frac{C_{p,a} - C_{\mathrm{control}}}{C_{\mathrm{control}}} \times 100$$

and

$$S_{c,p,a} = \frac{D_{c,p,a} - D_{c,p,-a}}{2a} \times 100,$$

where $C_{p,a}$ is the value of biomarker c when the parameter p is varied by the percentage a, and C_{control} is the value of biomarker c under control conditions. As shown above, sensitivity ($S_{c,p,a}$) was calculated as the ratio of the difference between the percentage of change ($D_{c,p,a} - D_{c,p,-a}$) and the interval of change ($2a$). In this study, we used this definition particularized for $a = 30\%$:

$$S_{c,p,30} = \frac{D_{c,p,+30} - D_{c,p,-30}}{0.6}.$$

Larger percentages of variation (±60% and ±90%) in model parameters were additionally investigated to confirm the validity of the sensitivity analysis results under more severe ionic alterations.

(ii) *Potassium current blocks*

The following cases of total and partial potassium current blocks were simulated.

— I_{Ks}: to simulate the effect of 1 µM of HMR-1556, I_{Ks} was completely blocked.
— I_{Kr}: to simulate the effect of 50 nM of dofetilide, I_{Kr} was completely blocked.
— I_{K1}: to simulate the effect of 10 µM of $BaCl_2$, I_{K1} was reduced by 50 per cent.

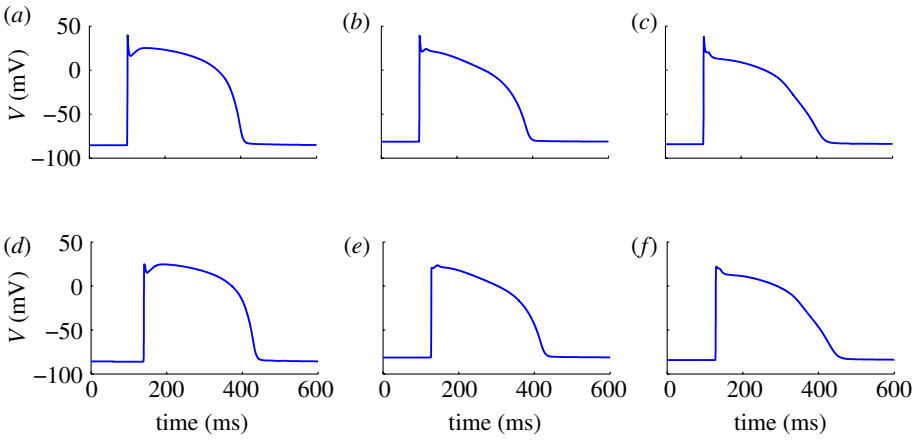

Figure 3. APs computed with the TP06, GPB and CRLP models for (*a–c*) isolated cells and (*d–f*) one-dimensional fibre tissue at CL = 1000 ms: (*a*) TP06 cellular AP; (*b*) GPB cellular AP; (*c*) CRLP cellular AP; (*d*) TP06 tissue AP; (*e*) GPB tissue AP; and (*f*) CRLP tissue AP. (Online version in colour.)

(iii) *Restitution in tissue*

CV and APD_{90} restitution were additionally investigated in tissue by applying the S1S2 protocol described in §2*b*(ii), with the only difference that the extra stimulus (S2) was in this case decreased in steps of 5 ms.

(iv) *Hyperkalaemic conditions*

Hyperkalaemic conditions were simulated by increasing $[K^+]_o$ from 4 to 15 mM. For each $[K^+]_o$ value, the diastolic threshold used to compute the stimulus amplitude was determined as follows: The model was first stabilized until the product of the gates $h \times j$ reached 99 per cent of the steady-state value $h_{ss} \times j_{ss}$. Stimulation current pulses of variable amplitude were applied at one end of the cable, and the diastolic threshold was defined as the minimum amplitude required for an AP to propagate along the fibre. With the model initialized at 1 Hz steady state, ERP was determined by stimulating the tissue with a train of 10 basic stimulations (S1) delivered at a CL of 1000 ms, followed by an extra stimulus (S2) delivered at different times taken in 1 ms steps. Steady-state CV and APD_{90} were measured after the last S1 stimulus.

3. Results

(*a*) *Results for control conditions*

(i) *APs in cell and tissue*

Figure 3 presents APs computed from the TP06, GPB and CRLP models for an isolated epicardial cell and for an epicardial cell coupled in tissue. In all cases, APs correspond to steady-state pacing at CL = 1000 ms. As can be appreciated from the figure, the AP duration is of the same order in the three models. However, the

Table 2. Results of the sensitivity analysis applied to the GPB model. The blue scale indicates relative sensitivity for each biomarker. White colour indicates maximum relative sensitivity and dark blue colour indicates that property and parameter are independent. Percentages in the white boxes indicate the absolute sensitivity of the property. A minus sign in a box indicates that biomarker and model parameter vary inversely. 'sys' stands for systolic and 'dia' stands for diastolic. (Online version in colour.)

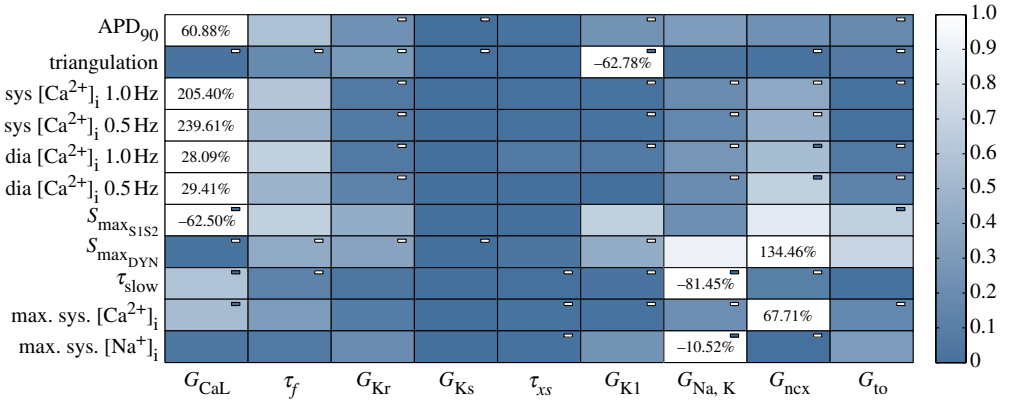

AP shape is notably more triangular for the GPB and the CRLP models when compared with the TP06 model, which presents a flatter plateau phase. Also, phase 1 of the AP substantially differs from one model to another, particularly when comparing TP06 with the other two models. Those differences are to some extent attenuated when comparing APs measured in tissue. It is also clear from the figure that maximal upstroke velocity is considerably reduced for tissue APs when compared with cell APs. While for the GPB and CRLP models, maximum voltage occurs at the upstroke peak in both cell and tissue, for the TP06 model, the maximum voltage at the plateau is even larger than at the upstroke peak in tissue AP, as previously noted by Bueno-Orovio *et al.* [6] for the TNNP04 model from which the TP06 model was developed.

(ii) *Sensitivity analysis*

The results of the sensitivity analysis applied to the epicardial version of the GPB model are presented in table 2. This table shows the dependence of a large number of arrhythmic risk biomarkers on the I_{CaL} current. Not only biomarkers related to systolic and diastolic $[Ca^{2+}]_i$ levels, but also APD_{90} and S1S2 restitution slope are mostly sensitive to variations in I_{CaL}. Also, table 2 shows the importance of the I_{K1} current for AP triangulation. $I_{Na,K}$ is determinant for $[Na^+]_i$ rate dependence as well as for the time constant of the slow phase of APD_{90} rate adaptation. Note that APD_{90} rate adaptation dynamics computed from the GPB model do not present a characteristic biphasic behaviour as reported in experimental studies [38], but adaptation is completed in only one slow phase. For that reason, the biomarker τ_{fast} described in §2*b*(i) is not shown in table 2. Finally, I_{ncx} is relevant for $[Ca^{2+}]_i$ rate dependence. Table 2 together

Table 3. Biomarkers of arrhythmic risk for the TP06, GPB and CRLP human models. Normal font indicates within physiological range. **Bold font** indicates out of physiological range but better than previous models. *Italic font* indicates out of physiological range. Experimental data are from earlier studies [14,17,25,38–43].

biomarker	TP06	GPB	CRLP	physiological
APD_{90} (ms)	301.2	285.0	305.6	271–366
triangulation (ms)	*28.4*	51.5	78	44–112
sys $[Ca^{2+}]_i$ 1 Hz (μM)	*0.886*	*0.383*	*0.602*	1.59–2.01
sys $[Ca^{2+}]_i$ 0.5 Hz (μM)	*0.199*	**0.345**	**0.523**	0.71–1.68
dia $[Ca^{2+}]_i$ 1 HZ (μM)	*0.104*	*0.089*	*0.097*	0.20–0.33
dia $[Ca^{2+}]_i$ 0.5 Hz (μM)	*0.068*	**0.085**	**0.091**	0.14–0.32
$S_{max_{S1S2}}$ (—)	1.3	*0.2*	1.0	0.79–4.25
$S_{max_{DYN}}$ (—)	1.0	1.1	0.9	—
τ_{fast} (s)	13.3	—	10.2	—
τ_{slow} (s)	*124.8*	*56.3*	105.6	70–110
max. sys. $[Ca^{2+}]_i$ (%)	*1157*	**178**	147	130–170
max. sys. $[Na^{+}]_i$ (%)	*217*	**132**	**134**	145

with the validation analysis presented in the following subsection were the road map to carry out the various model improvements proposed in this work, which were described in §2*a*.

To confirm that the results of the sensitivity analysis presented in table 2 were not dependent on the limit (30%) considered for parameter variations, simulations were performed considering larger percentages of variations of up to 90 per cent. Despite the fact that, in some cases, a highly nonlinear modulation of specific risk biomarkers by certain ionic mechanisms was observed (e.g. triangulation modulation by G_{K1}, systolic $[Ca^{2+}]_i$ modulation by G_{CaL} or τ_{slow} modulation by $G_{Na,K}$), the results corroborated the mechanisms identified as determinant for the investigated risk biomarkers in the sensitivity analysis.

(iii) *Arrhythmic risk biomarkers*

Table 3 shows the values of the computed biomarkers for the epicardial versions of the three models analysed in this study (TP06, GPB and CRLP). Simulation results were compared against a variety of experimental data taken from earlier studies [14,17,25,38–43].

Results indicate that the GPB model performs better than the TP06 model with respect to the following biomarkers: AP triangulation, steady-state systolic and diastolic $[Ca^{2+}]_i$ levels at 0.5 Hz, and rate dependence of $[Na^{+}]_i$ and $[Ca^{2+}]_i$. Those biomarkers are illustrated for the three analysed models in figure 4*a–g*. However, according to other analysed biomarkers, the GPB model renders worse performance than the TP06 model, as is the case for the S1S2 restitution curve and the APD_{90} adaptation to abrupt changes in CL. Regarding the APD_{90} adaptation, two phases of APD_{90} rate adaptation were experimentally reported in the study of Franz *et al.* [38]: a first phase with a short time constant and a second phase with a longer time constant. As described in §3*a*(ii), the APD_{90} rate response in the GPB model does not present the first fast phase

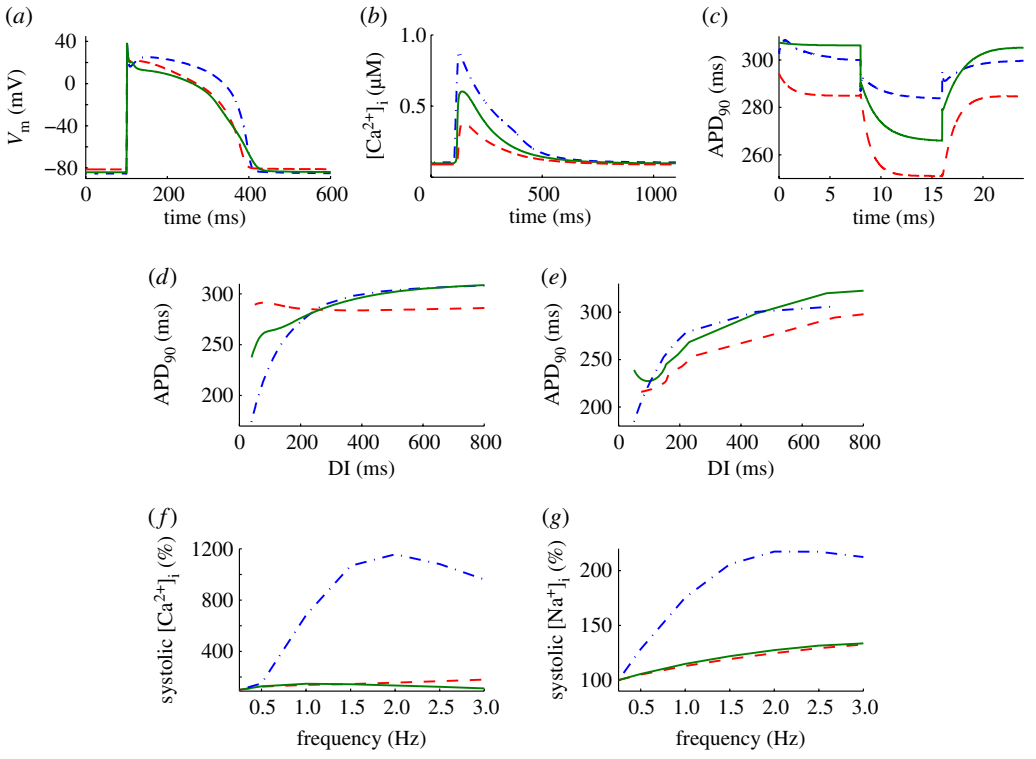

Figure 4. Biomarkers of arrhythmic risk from TP06, GPB and CRLP models: (*a*) steady-state AP for CL = 1000 ms; (*b*) steady-state $[Ca^{2+}]_i$ transient for CL = 1000 ms; (*c*) APD_{90} rate adaptation to abrupt changes in CL (from 1000 ms to 600 ms); (*d*) S1S2 restitution curve; (*e*) dynamic restitution curve; (*f*) normalized $[Ca^{2+}]_i$ rate dependence; and (*g*) normalized $[Na^+]_i$ rate dependence. (*f*,*g*) Normalization is performed with respect to the lowest tested frequency, i.e. 0.25 Hz. Red dashed line, GPB; green full line, CRLP; blue dashed-dotted line, TP06. (Online version in colour.)

(figure 4*c*). For the S1S2 restitution curves (figure 4*d*), the TP06 model is in better agreement with the experimental data of earlier studies [38,42] than the GPB model.

For the CRLP model, seven out of 12 analysed biomarkers are within physiological range and the other three are closer to the physiological range when compared with the GPB and the TP06 models. As for systolic and diastolic $[Ca^{2+}]_i$ levels at 1 Hz, TP06 outperforms CRLP. A significant change in the shape of the S1S2 restitution curve is observed for the CRLP model when compared with the GPB model (figure 4*d*). The behaviour shown by the CRLP model is in agreement with the experimental data [38].

(iv) *Potassium current blocks*

Table 4 summarizes the effect of potassium current blocks on epicardial APs computed using the three tested models. Results are given as percentage of variation of the APD_{90} value with respect to control conditions. In those cases where more than one current was blocked, the variation refers to the APD_{90} value

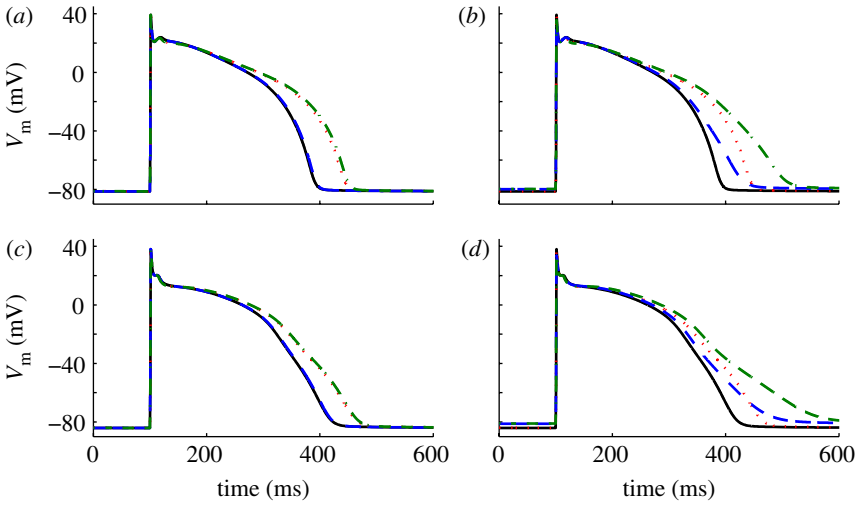

Figure 5. Effect of blocking potassium currents for the GPB and CRLP models. (*a*) Effect of completely blocking I_{Kr} and I_{Ks} currents in the GPB model (black solid line, control; red dotted line, I_{Kr} block; blue dashed line, I_{Ks} block; green dashed-dotted line; I_{Kr} and I_{Ks} block). (*b*) Effect of completely blocking I_{Kr} and partially blocking I_{K1} in the GPB model (black solid line, control; red dotted line, I_{Kr} block; blue dashed line, I_{K1} block; green dashed-dotted line; I_{Kr} and I_{K1} block). (*c*) Effect of completely blocking I_{Kr} and I_{Ks} currents in the CRLP model (black solid line, control; red dotted line, I_{Kr} block; blue dashed line, I_{Ks} block; green dashed-dotted line; I_{Kr} and I_{Ks} block). (*d*) Effect of completely blocking I_{Kr} and partially blocking I_{K1} in the CRLP model (black solid line, control; red dotted line, I_{Kr} block; blue dashed line, I_{K1} block; green dashed-dotted line; I_{Kr} and I_{K1} block). (Online version in colour.)

Table 4. Percentages of variation in APD_{90} caused by blocking different potassium currents. Normal font indicates within physiological range. **Bold font** indicates out of physiological range but better than previous models. *Italic font* indicates out of physiological range.

current		reference	TP06	GPB	CRLP	experiments
I_{Ks}	0%	control	*74.9*	0.7	0.6	<2.8
I_{Kr}	0%	control	*15.9*	**18.6**	*14.1*	44 ± 4
I_{Kr}	0%	I_{Kr} block	—	**1.4**	*0.8*	9
I_{Ks}	0%					
I_{K1}	50%	control	3.6	*11.5*	*14.6*	4.8 ± 1.5
I_{Kr}	0%	I_{Kr} block	*8.9*	**15.6**	**21.1**	33
I_{K1}	50%					

obtained when only the first current was blocked. Experimental values are taken from the study of Jost *et al.* [44]. It is clear from table 4 that the GPB model performs better than the TP06 model regarding current blocks. The CRLP model performs similar to the GPB model. Figure 5 illustrates the effect of current blocks on the AP shape for the GPB and CRLP models.

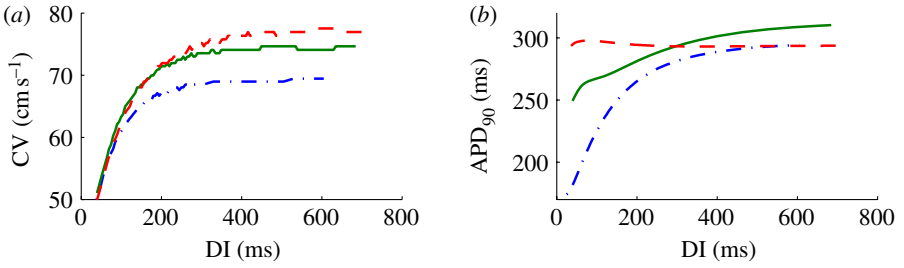

Figure 6. (*a*) CV and (*b*) APD_{90} restitution curves for the TP06, GPB and CRLP models in a simulated one-dimensional fibre. Blue dashed-dotted line, TP06; green solid line, CRLP; red dashed line, GPB. (Online version in colour.)

(v) *Restitution in fibre*

Figure 6 shows CV and APD_{90} restitution curves computed by applying the S1S2 protocol to the simulated one-dimensional fibre. Regarding CV restitution, the three models present similar behaviours, with only notable differences (greater than $5\,cm\,s^{-1}$) observed between the TP06 model and the other two models (GPB and CRLP) in the final part of the curve, i.e. for DI values above 200 ms. Regarding APD_{90} restitution, both the TP06 and CRLP models present steep restitution curves, with high slope (close to 1) only for a narrow DI interval in the case of the CRLP model and for a much wider DI range in the case of the TP06 model (with slope values above 1). The GPB model shows a relatively flat APD_{90} restitution curve. Those results are in good correspondence with the observations from restitution curves measured in isolated cells (figure 4*d*).

(*b*) *Results for hyperkalaemic conditions*

(i) *Action potential properties*

Figure 7*a,c* shows a comparison of the AP shape computed in a single cell and tissue for different levels of $[K^+]_o$ using the CRLP model. Figure 7*b,d* shows the effect of varying $[K^+]_o$ on the resting potential in a single cell and tissue. As expected, hyperkalaemia shortens the APD_{90} and leads to elevated resting potential, in both single cells and tissue.

From figure 7*c*, it is also clear that, for high $[K^+]_o$ levels, the AP shape varies between even and odd beats, thus leading to the occurrence of AP alternans. Further analysis on the alternating AP behaviour and the $[K^+]_o$ threshold for its occurrence can be found in §3*b*(iii).

(ii) *Conduction velocity*

Figure 8*a* shows CV as a function of $[K^+]_o$ computed from the simulated one-dimensional fibre using the CRLP model. As expected, hyperkalaemia leads to a decrease in CV. However, 'supernormal conduction' is not observed for $[K^+]_o$ levels below physiological values (5.4 mM) as has been observed in other studies [45,46]. Our results also show that conduction block occurs for $[K^+]_o > 10.4$.

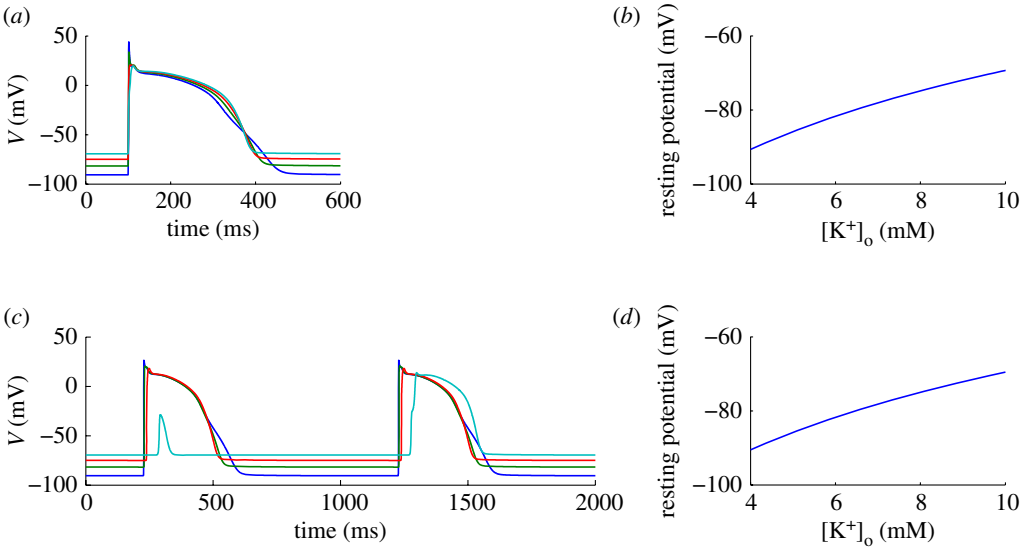

Figure 7. Simulated hyperkalaemia in (*a*,*b*) isolated cells and (*c*,*d*) one-dimensional fibre tissue using the CRLP model: (*a*) AP shape for varying $[K^+]_o$ (dark blue, 4; green, 6; red, 8; light blue, 10) in isolated cells; (*b*) resting potential for varying $[K^+]_o$ in isolated cells; (*c*) AP shape for varying $[K^+]_o$ (dark blue, 4; green, 6; red, 8; light blue, 10) in one-dimensional fibre; and (*d*) resting potential for varying $[K^+]_o$ in one-dimensional fibre. (Online version in colour.)

(iii) *Action potential duration and effective refractory period*

Figure 8*b* shows ERP and APD_{90} of the last basic (S1) beat for different $[K^+]_o$ values computed in the simulated one-dimensional fibre using the CRLP model. Results show that hyperkalaemia causes post-repolarization refractoriness. The difference between ERP and APD_{90} remains almost constant for $[K^+]_o \leq 6$ mM, with this difference increasing rapidly for $[K^+]_o > 6$ mM. For $[K^+]_o > 9.8$ mM, alternans appear in the tissue, causing the ERP and APD_{90} curves to branch out (figure 8*b*). This characteristic of the ERP and APD_{90} curves has not been reported in other human ventricular simulation studies of the literature, but is in agreement with the experimental results in other species and with clinical data [47–49]. We tested the same hyperkalaemic conditions in simulated TP06 and GPB one-dimensional fibres and we could not observe branching out of the ERP or APD_{90} curves after increasing $[K^+]_o$ up to 15 mM.

Figure 8*c* depicts AP propagation in the simulated CRLP one-dimensional fibre for $[K^+]_o = 10$ mM. Alternans were observed for all computed positions within the fibre. Figure 8*d* shows I_{CaL}, I_{Na} and $[Ca^{2+}]_i$, each normalized to its maximum value, for the same time period shown in figure 8*c*. Results indicate that conduction relies on I_{Na} even for the highly depressed APs. For the long APs, the AP upstroke is divided into two components, the first one characterized by a steep upstroke and supported by I_{Na}, and the second one supported by I_{CaL}, in agreement with the results reported in [50].

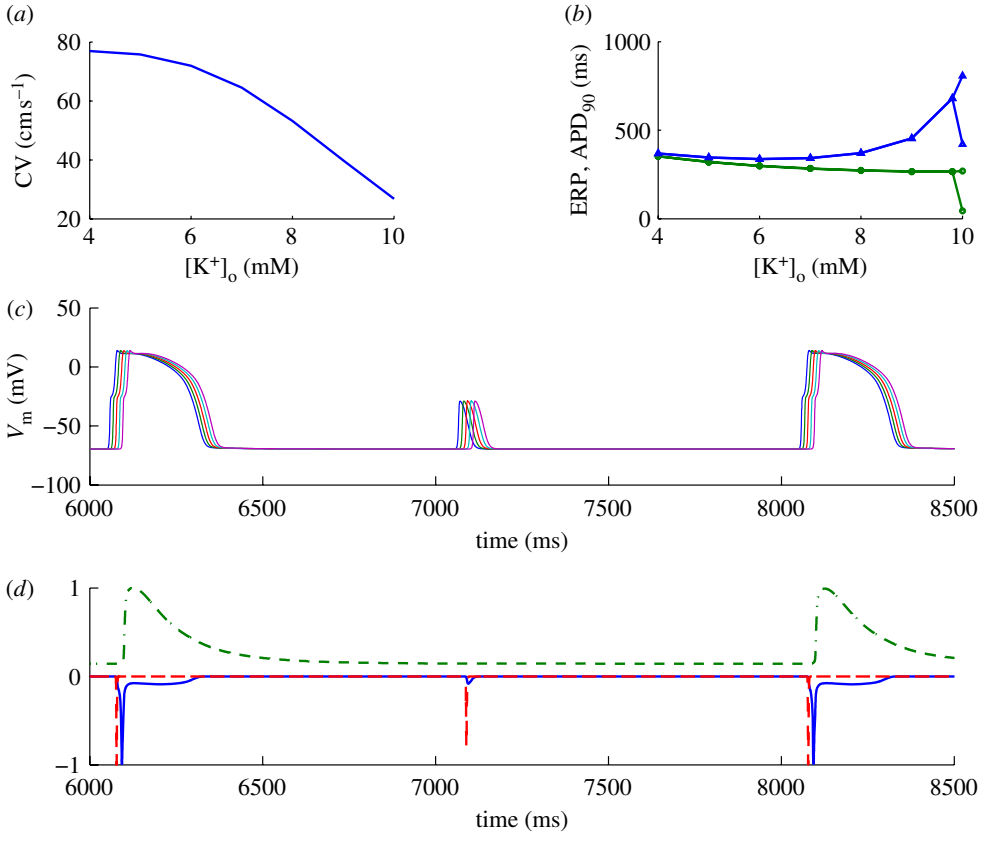

Figure 8. Behaviour of the CRLP model under hyperkalaemic conditions in a one-dimensional fibre: (*a*) CV versus $[K^+]_o$; (*b*) dependence of ERP (blue line with filled triangles) and APD_{90} (green line with filled circles) with $[K^+]_o$; (*c*) example of alternans for $[K^+]_o = 10.0$ mM, each colour representing a different position in the fibre; and (*d*) value of different currents normalized to the maximal value of each one in the same example as the previous results (blue full line, I_{CaL}; red dashed line, I_{Na}; green dashed-dotted line, $[Ca^{+2}]_i$). (Online version in colour.)

4. Discussion and conclusions

In this study, a new human ventricular cell model, the CRLP model, was developed based on the recently proposed GPB model. The CRLP model combines recent experimental measurements of potassium currents, and reformulates the L-type calcium current by introducing fast and slow voltage-dependent inactivation gates, similar to the formulation proposed in the TP06 model. That new formulation led to I_{CaL} dynamics that were in good agreement with experimental data and, more notably, allowed the CRLP model to accurately reproduce S1S2 restitution and APD_{90} rate adaptation characteristics. All the modifications were made with the aim of maintaining the advantages that the GPB model has over previous models, such as the TP06 model, while improving the performance on other electrophysiological aspects. The novelty of this study was that model development was not only based on the incorporation

of new data from experiments on individual ionic currents or concentrations. More importantly, the development was driven by analysing the ability of the model to replicate a set of well-established arrhythmic risk biomarkers, and on a sensitivity analysis of those biomarkers to variations in model parameters. The proposed model development framework allows model performance to be assessed under a variety of conditions, either physiological or pathological. This provides useful information for the adjustment of different model parameters that do not directly depend on individual current measurements or concentrations, and which would otherwise be set in an *ad hoc* manner.

(*a*) *Modifications*

The introduction of fast and slow I_{CaL} inactivation gates in the CRLP model led to a more physiological APD_{90} rate adaptation response to abrupt changes in CL when compared with the GPB model. However, by doing so, a larger I_{CaL} current was obtained for the CRLP model, which led to the reformulation of I_{K1} and readjustments of other parameters in order to keep APD_{90} within physiological values. The resulting APD_{90} value for the CRLP model was closer to the APD_{90} value of the TP06 model, without significantly altering the AP triangulation of the GPB model, which was well within the reported physiological range. The other modifications introduced into the CRLP model rendered most of the investigated biomarkers to be within the physiological range or otherwise closer to the physiological range when compared with the GPB and the TP06 models. In this regard, it was only for systolic and diastolic $[Ca^{2+}]_i$ levels at 1 Hz that TP06 outperformed CRLP. In addition, the CRLP model showed improved performance with respect to the GPB model regarding the S1S2 restitution, not only by bringing the maximum S1S2 restitution slope within the physiological range, but also by providing a shape for the restitution curve in good agreement with the experimental measurements [38].

Even though the modifications significantly improved the performance of the CRLP model over the GPB model in reproducing experimental data related to a number of arrhythmic risk biomarkers, they have minimally affected the behaviour of the model against potassium current blocks. In this regard, the CRLP model still provides results in very good agreement with the available experimental data regarding AP response to I_{Kr}, I_{Ks} and I_{K1} blocks [44].

(*b*) *Simulation of hyperkalaemic conditions*

Simulations under hyperkalaemic conditions showed that APD_{90} progressively decreased with the level of $[K^+]_o$, whereas ERP increased after a threshold was reached ($[K^+]_o \approx 6$ mM) in $[K^+]_o$. CV decreased with hyperkalaemia and conduction was blocked above $[K^+]_o = 10.4$ mM. These results suggest that the longer ERP values and the occurrence of conduction block above $[K^+]_o = 10.4$ mM in the central zone of acute ischaemic tissue could cause areas of conduction block that could set a substrate for reentrant arrhythmias. Additionally, alternans were observed in ERP and APD_{90} for $[K^+]_o > 9.8$ mM. These results are in agreement with experimental studies, where alternans were observed in the cells of the heart's ischaemic zone [47,48]. To the authors' knowledge, this is the first time that those observations have been reported using a human ventricular AP model. That type of behaviour was not observed in either the TP06 or the GPB models.

For the TP06 model, conduction block occurred for $[K^+]_o \approx 15$ mM without the occurrence of alternans [51]. For the GPB model, conduction block occurred for $[K^+]_o \approx 9$ mM and alternans were not observed either.

(c) Data sources

As described in the study of Niederer *et al.* [3], one of the problems on reutilization of model components in electrophysiology is the inclusion of components adjusted with data from different species. For that reason, in this work all the modifications were made by using model components formulated based on human data only [1] or by fitting equations to additional human data available from the literature [9]. We did not try modifying other ionic currents or concentrations for which human data were not available. Regarding the types of human data used in the study, they all corresponded to adult humans, except for the data taken from the study by Pelzmann *et al.* [15], in which I_{CaL} was measured in children. Those data were used because the study clearly showed that there were not significant differences in the I_{CaL} current characteristics measured in children when compared with adults.

(d) Model limitations

The developed CRLP model has a number of limitations, some of them inherited from the GPB model on which it was based, and others independent of it. Phase 1 of the AP shows an atypical behaviour. We believe this behaviour is caused by the I_{to} current. However, we have not attempted to modify this current mainly because new human data were not available for that purpose. This current happens to be the only one whose definition differentiates endocardial and epicardial cells in the GPB model and in the CRLP model as well. A second limitation of the CRLP model, which is also a limitation of the GPB model, is that a description is not provided for the electrophysiology of mid-myocardial cells. Another limitation of the CRLP model has to do with calcium definition. The results of the analysis conducted in this study point out the importance that the I_{CaL} current as well as the $[Ca^{2+}]_i$ dynamics have over different arrhythmic risk biomarkers. Many studies have attempted to provide accurate definitions of $[Ca^{2+}]_i$ dynamics in human ventricular cells, but this is still an area of intensive research. The present study suggests the need to continue with the development of more reliable calcium dynamics models that allow the performance of whole-cell AP models to be improved.

On top of the above-described limitations, a comment is in order regarding the comparison of human ventricular AP models. It is clear that each model has been developed to reproduce certain electrophysiological behaviours observed from experimental recordings. Also, considering the huge variability in the experimental data, model comparison becomes a challenging task for which a model should never be qualified as being an improvement over another one just because it is able to reproduce specific experimental observations that the other model is not able to. In this study, we used the term ‘improvement’ exclusively to refer to the fact that, considering the set of investigated arrhythmic risk biomarkers, the CRLP model provides a response that is more in line with the averaged experimental data used for evaluation purposes.

(*e*) *Future work*

Although the results of this study showed the value of the proposed framework for the development of ionic models, further research is needed to investigate how arrhythmic risk biomarkers are modulated by the interaction of different model parameters when those parameters vary simultaneously. In this regard, an analysis of variance of the studied biomarkers can provide additional useful information for adjusting independent parameters in order to bring a given biomarker into the physiological range without greatly affecting other biomarkers in the process. Future developments of the model will continue in this direction, as well as in adapting the model for simulating ischaemia through the incorporation of ATP-sensitive potassium channels (I_{KATP}). Simulations with the CRLP model will be conducted not only in a one-dimensional fibre, but in two-dimensional tissue and in a realistic human ventricular geometry.

This study was financially supported by grants TEC2010-19410 and TEC2010-21703-C03-02 from Ministerio de Ciencia e Innovación, Spain, PI 144/2009 and Grupo Consolidado T30 from Gobierno de Aragón, Spain, an International Joint Project from the Royal Society, UK, and fellowship B040/2010 from Gobierno de Aragón, Spain. The authors would like to thank Eleonora Grandi for sharing the codes of the GPB model before making them available at the CellML repository.

References

1 ten Tusscher, K. & Panfilov, A. 2006 Alternans and spiral breakup in a human ventricular tissue model. *Am. J. Physiol. Heart Circ. Physiol.* **291**, H1088–H1100. (doi:10.1152/ajpheart.00109.2006)

2 ten Tusscher, K., Noble, D., Noble, P. J. & Panfilov, A. 2004 A model for human ventricular tissue. *Am. J. Physiol. Heart Circ. Physiol.* **286**, H1573–H1589. (doi:10.1152/ajpheart.00794.2003)

3 Niederer, S., Fink, M., Noble, D. & Smith, N. 2009 A meta-analysis of cardiac electrophysiology computational models. *Exp. Physiol.* **94**, 486–495. (doi:10.1113/expphysiol.2008.044610)

4 Romero, L., Pueyo, E., Fink, M. & Rodríguez, B. 2009 Impact of ionic current variability on human ventricular cellular electrophysiology. *Am. J. Physiol. Heart Circ. Physiol.* **297**, H1436–H1445. (doi:10.1152/ajpheart.00263.2009)

5 Iyer, V., Mazhari, R. & Winslow, R. 2004 Computational model of the human left ventricular epicardial myocyte. *Biophys. J.* **87**, 1507–1525. (doi:10.1529/biophysj.104.043299)

6 Bueno-Orovio, A., Cherry, E. M. & Fenton, F. H. 2008 Minimal model for human ventricular action potentials in tissue. *J. Theor. Biol.* **253**, 544–560. (doi:10.1016/j.jtbi.2008.03.029)

7 Grandi, E., Pasqualini, F. S. & Bers, D. M. 2010 A novel computational model of the human ventricular action potential and Ca transient. *J. Mol. Cell. Cardiol.* **48**, 112–121. (doi:10.1016/j.yjmcc.2009.09.019)

8 Shannon, T. R., Wang, F., Puglisi, J., Weber, C. & Bers, D. M. 2004 A mathematical treatment of integrated Ca dynamics within the ventricular myocyte. *Biophys. J.* **87**, 3351–3371. (doi:10.1529/biophysj.104.047449)

9 Fink, M., Noble, D., Virag, L., Varro, A. & Giles, W. R. 2008 Contributions of HERG K^+ current to repolarization of the human ventricular action potential. *Prog. Biophys. Mol. Biol.* **96**, 357–376. (doi:10.1016/j.pbiomolbio.2007.07.011)

10 Beuckelmann, D. J., Näbauer, M. & Erdmann, E. 1991 Characteristics of calcium-current in isolated human ventricular myocytes from patients with terminal heart failure. *J. Mol. Cell. Cardiol.* **23**, 929–937. (doi:10.1016/0022-2828(91)90135-9)

11 Benitah, J., Bailly, P., D'Agrosa, M., Da Ponte, J., Delgado, C. & Lorente, P. 1992 Slow inward current in single cells isolated from adult human ventricles. *Pflügers Arch.* **421**, 176–187. (doi:10.1007/BF00374825)

12 Mewes, T. & Ravens, U. 1994 L-type calcium currents of human myocytes from ventricle of non-failing hearts and atrium. *J. Mol. Cell. Cardiol.* **26**, 1307–1320. (doi:10.1006/jmcc.1994.1149)
13 Sun, H., Leblanc, N. & Nattel, S. 1997 Mechanisms of inactivation of L-type calcium channels in human atrial myocytes. *Am. J. Physiol. Heart Circ. Physiol.* **272**, H1625–H1635.
14 Li, G. R., Yang, B., Feng, J., Bosch, R. F., Carrier, M. & Nattel, S. 1999 Transmembrane I_{Ca} contributes to rate-dependent changes of action potentials in human ventricular myocytes. *Am. J. Physiol. Heart Circ. Physiol.* **276**, H98–H106.
15 Pelzmann, B., Schaffer, P., Bernhart, E., Lang, P., Machler, H., Rigler, B. & Koidl, B. 1998 L-type calcium current in human ventricular myocytes at a physiological temperature from children with tetralogy of Fallot. *Cardiovasc. Res.* **38**, 424–432. (doi:10.1016/S0008-6363(98)00002-9)
16 Magyar, J. *et al.* 2000 Effects of endothelin-1 on calcium and potassium currents in undiseased human ventricular myocytes. *Pflügers Arch.* **441**, 144–149. (doi:10.1007/s004240000400)
17 Drouin, E., Charpentier, F., Gauthier, C., Laurent, K. & Marec, H. L. 1995 Electrophysiologic characteristics of cells spanning the left ventricular wall of human heart: evidence for presence of M cells. *J. Am. Coll. Cardiol.* **26**, 185–192. (doi:10.1016/0735-1097(95)00167-X)
18 Hodgkin, A. L. & Huxley, A. F. 1952 A quantitative description of ion currents and its applications to conduction and excitation in nerve membranes. *J. Physiol.* **117**, 500–544.
19 Keener, J. & Sneyd, J. 1998 *Mathematical physiology.* Berlin, Germany: Springer.
20 Heidenreich, E., Ferrero, J. M., Doblaré, M. & Rodríguez, J. F. 2010 Adaptive macro finite elements for the numerical solution of monodomain equations in cardiac electrophysiology. *Ann. Biomed. Eng.* **38**, 2331–2345. (doi:10.1007/s10439-010-9997-2)
21 Taggart, P., Sutton, P., Opthof, T., Coronel, R., Trimlett, R. & Pugsley, W. 2000 Inhomogeneous transmural conduction during early ischemia in patients with coronary artery disease. *J. Mol. Cell. Cardiol.* **32**, 621–639. (doi:10.1006/jmcc.2000.1105)
22 Rush, S. & Larsen, H. 1978 A practical algorithm for solving dynamic membrane equations. *IEEE Trans. Biomed. Eng.* **25**, 389–392. (doi:10.1109/TBME.1978.326270)
23 Hondeghem, L., Carlsson, L. & Duker, G. 2001 Instability and triangulation of the action potential predict serious proarrhythmia, but action potential duration prolongation is antiarrhythmic. *Circulation* **103**, 2004–2013. (doi:10.1161/01.CIR.103.15.2004)
24 Volders, P., Vos, M., Szabo, B., Sipido, K., de Groot, S., Gorgels, A., Wellens, H. & Lazzara, R. 2000 Progress in the understanding of cardiac early afterdepolarizations and torsades de pointes: time to revise current concepts. *Cardiovasc. Res.* **46**, 376–392. (doi:10.1016/S0008-6363(00)00022-5)
25 Pieske, B., Maier, L., Bers, D. & Hasenfuss, G. 1999 Ca^{2+} handling and sarcoplasmic reticulum Ca^{2+} content in isolated failing and nonfailing human myocardium. *Circ. Res.* **85**, 38–46.
26 Bers, D. M. & Despa, S. 2006 Cardiac myocytes Ca^{2+} and Na^{+} regulation in normal and failing hearts. *J. Pharmacol. Sci.* **100**, 315–322. (doi:10.1254/jphs.CPJ06001X)
27 Pueyo, E., Smetana, P., Caminal, P., de Luna, A., Malik, M. & Laguna, P. 2004 Characterization of QT interval adaptation to RR interval changes and its use as a risk-stratifier of arrhythmic mortality in amiodarone-treated survivors of acute myocardial infarction. *IEEE Trans. Biomed. Eng.* **51**, 1511–1520. (doi:10.1109/TBME.2004.828050)
28 Pueyo, E., Husti, Z., Hornyik, T., Baczkó, I., Laguna, P., Varró, A. & Rodríguez, B. 2010 Mechanisms of ventricular rate adaptation as a predictor of arrhythmic risk. *Am. J. Physiol. Heart Circ. Physiol.* **298**, H1577–H1587. (doi:10.1152/ajpheart.00936.2009)
29 Nolasco, J. & Dahlen, R. 1968 A graphic method for the study of alternation in cardiac action potentials. *J. Appl. Physiol.* **25**, 191–196.
30 Weiss, J., Karma, A., Shiferaw, U., Chen, P., Garfinkel, A. & Qu, Z. 2006 From pulses to pulseless: the saga of cardiac alternans. *Circ. Res.* **98**, 1244–1253. (doi:10.1161/01.RES.0000224540.97431.f0)
31 Levi, A. *et al.* 1997 Role of intracellular sodium overload in the genesis of cardiac arrhythmias. *J. Cardiovasc. Electrophysiol.* **8**, 700–721. (doi:10.1111/j.1540-8167.1997.tb01834.x)

32 Murphy, E. & Eisner, D. 2009 Regulation of intracellular and mitochondiral sodium in health and disease. *Circ. Res.* **104**, 292–303. (doi:10.1161/CIRCRESAHA.108.189050)

33 Fülöp, L., Bányász, T., Magyar, J., Szentandrássy, N., Varró, A. & Nánási, P. P. 2004 Reopening of L-type calcium channels in human ventricular myocytes during applied epicardial action potentials. *Acta Physiol. Scand.* **180**, 37–94. (doi:10.1046/j.0001-6772.2003.01223.x)

34 Iost, N., Virág, L., Opincariu, M., Szécsi, J., Varró, A. & Papp, J. G. 1998 Delayed rectifier potassium current in undiseased human ventricular myocytes. *Cardiovasc. Res.* **40**, 508–515. (doi:10.1016/S0008-6363(98)00204-1)

35 Szentadrassy, N. *et al.* 2005 Apico-basal inhomogeneity in distribution of ion channels in canine and human ventricular myocardium. *Cardiovasc. Res.* **65**, 851–860. (doi:10.1016/j.cardiores.2004.11.022)

36 Verkerk, A. O., Wilders, R., Veldkamp, M. W., de Geringel, W., Kirkels, J. H. & Tan, H. L. 2005 Gender disparities in cardiac cellular electrophysiology and arrhythmia susceptibility in human failing ventricular myocytes. *Int. Heart J.* **46**, 1105–1118. (doi:10.1536/ihj.46.1105)

37 Virág, L., Iost, N., Opincariu, M., Szolnoky, J., Szécsi, J., Bogáts, G., Szenohradszky, P., Varró, A. & Papp, J. 2001 The slow component of the delayed rectifier potassium current in undiseased human ventricular myocytes. *Cardiovasc. Res.* **49**, 790–797. (doi:10.1016/S0008-6363(00)00306-0)

38 Franz, M. R., Swerdlow, C. D., Liem, L. B. & Schaefer, J. 1988 Cycle length dependence of human action potential duration *in vivo*. Effects of single extrastimuli, sudden sustained rate acceleration and deceleration, and different steady-state frequencies. *J. Clin. Invest.* **82**, 972–979. (doi:10.1172/JCI113706)

39 Li, G. R., Feng, J., Yue, L. & Carrier, M. 1998 Transmural heterogeneity of action potentials and I_{to1} in myocytes isolated from the human right ventricle. *Am. J. Physiol. Heart Circ. Physiol.* **275**, H369–H377.

40 Beuckelmann, D. J., Nabauer, M. & Erdmann, E. 1992 Intracellular calcium handling in isolated ventricular myocytes from patients with terminal heart failure. *Circulation* **85**, 1046–1055.

41 Schmidt, U., Hajjar, R., Helm, P., Kim, C., Doye, A. & Gwathmey, J. 1998 Contribution of abnormal sarcoplasmic reticulum ATPase activity to systolic and diastolic dysfunction in human heart failure. *J. Mol. Cell. Cardiol.* **30**, 1929–1937. (doi:10.1006/jmcc.1998.0748)

42 Nash, M., Gradley, C., Sutto, P., Clayton, R., Kallis, P., Hayward, M., Paterson, D. & Taggart, P. 2006 Whole heart action potential duration restitution properties in cardiac patients: a combined clinical and modelling study. *Exp. Physiol.* **91**, 339–354. (doi:10.1113/expphysiol.2005.031070)

43 Pieske, B., Maier, L., Piacentino III, V., Weisser, J., Hasenfuss, G. & Houser, S. 2002 Rate dependence of $[Na^+]_i$ and contractility in nonfailing and failing human myocardium. *Circulation* **106**, 447–453. (doi:10.1161/01.CIR.0000023042.50192.F4)

44 Jost, N. *et al.* 2008 Molecular basis of repolarization reserve differences between dogs and man. *Circulation* **118**(Meeting Abstr. Suppl.), S342.

45 Shaw, R. M. & Rudy, Y. 1997 Electrophysiologic effects of acute myocardial ischemia: a mechanistic investigation of action potential conduction and conduction failure. *Circ. Res.* **80**, 124–138.

46 Kagiyama, Y., Hill, J. & Gettes, L. 1982 Interaction of acidosis and increased extracellular potassium on action potential characteristic and conduction in guinea pig ventricular muscle. *Circ. Res.* **51**, 614–623.

47 Dilly, S. G. & Lab, M. J. 1988 Electrophysiological alternans and restitution during acute regional ischaemia in myocardium of anaesthetized pig. *J. Physiol.* **402**, 315–333.

48 Kurz, R. W., Mohabir, R., Ren, X. L. & Franz, M. R. 1993 Ischaemia induced alternans of action potential duration in the intact-heart: dependence on coronary flow, preload and cycle length. *Eur. Heart J.* **14**, 1410–1420. (doi:10.1093/eurheartj/14.10.1410)

49 Martínez, J. P., Olmos, S., Wagner, G. & Laguna, P. 2006 Characterization of repolarization alternans during ischemia: time-course and spatial analysis. *IEEE Trans. Biomed. Eng.* **53**, 701–711. (doi:10.1109/TBME.2006.870233)

50 Ferrero, J. M., Trenor, B., Rodriguez, B. & Saiz, J. 2003 Electrical activity and reentry during acute regional myocardial ischemia: insights from simulations. *Int. J. Bifurc. Chaos* **13**, 3703–3715. (doi:10.1142/S0218127403008806)

51 Rodriguez, J., Heidenreich, E., Romero, L., Ferrero, J. & Doblare, M. 2008 Post-repolarization refractoriness in human ventricular cardiac cells. In *Computers in cardiology 2008, Bologna, Italy, 14–17 September*, vol. 35, pp. 581–584. Washington, DC: IEEE Computer Society Press. See http://www.cinc.org/archives/2008/pdf/0581.pdf.